View metadata, citation and similar papers at core.ac.uk
brought to you by CORE
provided by University of Liverpool Repository

RETINAL VASCULAR TOPOLOGY ESTIMATION VIA DOMINANT SETS CLUSTERING

XX

[1]Beijing Engineering Research Center of Mixed Reality and Advanced Display, School of Optics and Electronics, Beijing Institute of Technology, Beijing, China.

[2]Cixi Institute of Biomedical Engineering, Ningbo Institute of Industrial Technology, Chinese Academy of Sciences, Ningbo, China

[*]E-mail: yitian.zhao@nimte.ac.cn

ABSTRACT

The estimation of vascular topology in complex networks is important in understanding vascular changes. Automatic method of analysis of vascular networks would be of great assistance to the ophthalmologist in terms of diagnosis and treatment. In this paper, we propose a novel vessel topology estimation method based on the concept of *dominant sets clustering*. Dominant sets clustering is a graph-theoretic approach that has proven to work well in data clustering, and has been successfully adapted to topology estimation in this work. The experimental results show that it has addressed the bottleneck issue of vessel connection at crossovers, and yielded accuracy of 0.915, 0.928, and 0.889 on the IOSTAR, INSPIRE, and VICAVR databases, respectively. It is worth noting that we have made manual annotations of vessel topologies from these databases, and these annotations will be released soon.

***Index Terms*—** Dominant sets, topology, retinal vessel, graph.

1. INTRODUCTION

Automated analysis of retinal vascular structure is very important for many clinical applications to support examination, diagnosis and treatment of eye disease. This has the potential to perform automated screening for pathological conditions, and to provide crucial hints on various diseases [1, 2, 3, 4, 5], in particular diabetic retinopathy (DR), malaria retinopathy (MR), glaucoma, and hypertensive retinopathy.

The above-mentioned diseases always cause vascular abnormalities. Amongst these are variations in vascular width and changes in vascular tortuosity. It is often crucial to identify the structure of individual vessels from the entire retinal blood vessel network. This calls for proper description of vascular structure in terms of topological and geometrical properties from retinal images. Extensive work has been done on automatic vessel segmentation[1, 6, 7, 8, 9] and classification[4, 10, 11, 12, 13], but automated estimation of retinal vascular topology has received relatively limited attention. To the best of our knowledge, a small number of studies have addressed this subject directly.

A semi-automatic method of measuring and quantifying the topological properties of retinal vessels was proposed by Martinez-Perez et al.[14], which we consider to be the first work on retinal vascular topology estimation. Measurements of length, area, angles and connectivity between branches were taken to label the segmented vessel trees. Qureshi et al.[15] used a Bayesian approach to addressing the configuration of vascular junctions, and utilized a probabilistic model and Maximum A Posterior (MAP) to construct the vascular trees. Estrada et al.[16] regularized the topology estimation problem with a generative, parametric tree-growth model. A combination of greedy approximation and heuristic search algorithm was proposed to explore the space of possible trees. De et al.[3] proposed a graph-theoretical method to trace tree structures in neuronal and retinal images. The authors reformulated the topology estimation problem as label propagation over directed graphs: in this way the graph is decomposed into sub-graphs, and each vessel tree may be separated from the vessel network. Another graph-based approach for retinal vessel topology estimation was introduced by Dashtbozorg et al.[11]. They classified the entire vessel networks depending on the type of graph nodes and assigned one of two labels to each vessel fragment. These earlier proposed methods often fail to describe the presence of crossover at vessel junctions, as the measurements of caliber are unreliable at abrupt changes from one vessel to another of different bore.

The main contributions of this paper are as follows. First, we adapted the concept of dominant sets clustering [17, 18] to the task of vessel topology estimation, as it offers an efficient way of addressing problem of the tracing of crossovers. Second, the proposed method has been validated quantitatively using three publicly accessible datasets. Manual annotations of vessel topologies from these datasets were established, and these annotations will be released for public access.

2. METHOD

The proposed vessel topology estimation method relies on a prior vessel segmentation procedure, which may be performed manually or automatically. A skeletonlization method is then used to generate the vessel centreline map, and the

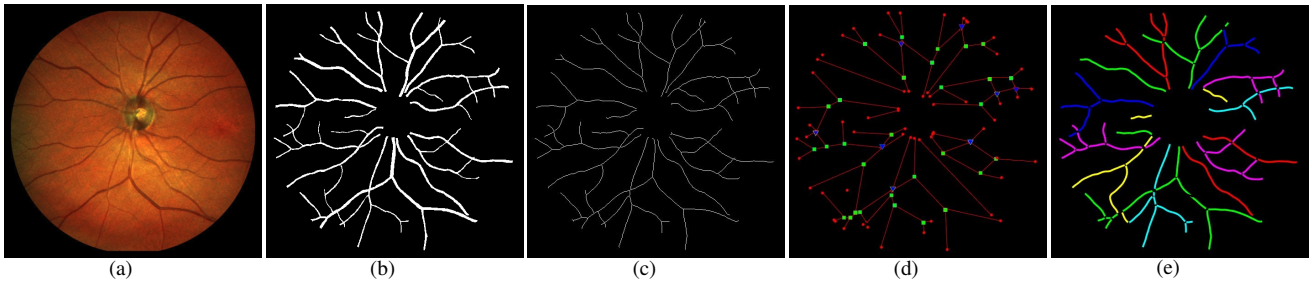

Fig. 1. Retinal vascular graph and topology construction. (a) Original color fundus image. (b) Segmentation result. (c) Skeleton map. (d) Generated graph with significant nodes. Red dots indicate the terminal points, green squares the bifurcations, and blue triangle the crossing and meeting points. (e) Our estimated vascular topology.

significant points, such as bifurcation, crossing, meeting and connecting points can be identified. These points are then utilized to create a graph. Finally, the dominant sets concept is used to classify the significant nodes, in order to estimate the vessel topology.

2.1. Vessel segmentation

In this work, our proposed topology estimation procedure is applied either on manual annotations or automated segmentation results. The method proposed by Zhao et al.[19] was employed to segment the retinal vessel automatically. This method uses an infinite perimeter active contour model for its effectiveness in detecting vessels with irregular and oscillatory boundaries, and it also considers hybrid region information in order to achieve further improved performance. Fig. 1 (b), above, demonstrates the segmentation result of Fig. 1 (a).

2.2. Graph generation

An iterative morphology thinning operation [20] is performed on the vessel segmentation results to obtain the single-pixel-wide skeleton map. The generated skeleton map is shown in Fig. 1 (c). The vascular bifurcation / crossover points, and vessel ends (connecting points) can be extracted from the skeleton map by locating intersection points (pixels with more than two neighbors) and terminal points (pixels with just one neighbor). All the intersection points and their neighbors may then be removed from the skeleton map, in order to obtain an image with clearly separated vessel segments. Finally, a vessel graph can be generated by linking first and last nodes in the same vessel segment, as shown as Fig. 1 (d).

2.3. Graph modification

However, the generated graph always includes misrespresentations of the vessels, and so it is important to modify this incorrect graph in order to avoid false classification of nodes. As summarized in [11], typical errors are *node splitting* and *false link*. The representation and modification of these two errors are as follows.

(1) *False link* is demonstrated in Fig. 2 (a): an incorrect link c between two nodes n_1 and n_2 is created. This happens when two vessels are close to each other, but do not cross. To resolve this case, the angles α and β between the edges connected to each node are computed. If the angles satisfy $\alpha_1, \alpha_2 \in (180^\circ \pm 10^\circ)$ and $\beta_1, \beta_2 \in (90^\circ \pm 10^\circ)$, then we consider link c to be a false link, which should be removed. Fig. 2 (c) demonstrates the corrected graph.

(2) *Node splitting* is illustrated in Fig. 2 (d): false nodes n_1 and n_2 are created. This happens when two vessels are close enough to cross each other. To address this problem, we define two angles α and β as shown in Fig. 2 (e). If the measured angles satisfy $\alpha_1, \alpha_2 < 60^\circ$ and $\beta_1, \beta_2 > 90^\circ$, this situation can be considered as an instance of node splitting, and edge c should be removed and the two neighborhood intersect point n_1 and n_2 merged as one node n. Fig. 2 (f) reveals the misrespresented graph is modified.

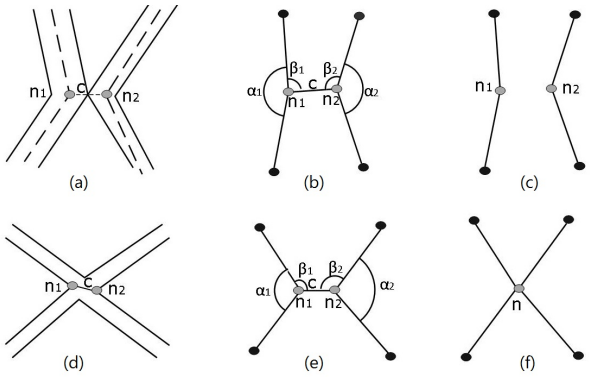

Fig. 2. The two types of graph modification. (a)(b) illustrate a false link, corrected at (c) to show two separate vessels, while (d)(e) illustrate node splitting, corrected at (f) to show a single node at an intersection.

2.4. Node Analysis

Node analysis is broken down into four cases (node degrees 2-5), based on four different types of nodes: connecting points (2), bifurcation points (3, 4), crossing points (4, 5), and meet-

ing points (3, 4, 5). The number in the bracket indicates the possible number of links connected to each node (node degree). The method proposed by Dashtbozorg et al.[11] is used to handle the cases of nodes of degree 2-3. For the more complicated cases, nodes of degree 4 and 5, a classification method based on dominant sets clustering is proposed. In this work, for each centerline pixel, the intensities in R, G, B channels, orientations, curvatures, and diameters of vessel are used as the input of the dominant sets clustering based classifier.

2.4.1. Dominant set clustering

The nodes to be classified are represented as an undirected edge-weighted graph with $G = (V, E, \omega)$, where the node set $V = \{1, \cdots, n\}$, and usually $n \leq 5$. The edge set $E \subseteq V \times V$ indicates all the possible connections. $\omega : E \rightarrow R_+^*$ is the positive weight function. Nodes in G correspond to vessel node ends: edges represent node relationships, and edge weight reveals similarity between pairs of linked nodes. The symmetric matrix $A = (a_{ij})$ is used to represent the graph G with weighted adjacency matrix. This non-negative adjacency matrix is defined as:

$$a_{ij} = \begin{cases} \omega(i,j) & \text{if } (i,j) \in E \\ 0 & \text{otherwise.} \end{cases} \tag{1}$$

Note: all elements on the main diagonal of A are zero, since G is self-loops free.

In general, the weights of edges within a vessel segment should be large, representing high internal homogeneity or similarity. By contrast, the weights of edges will be small for two or more different vessel segments, those on the edges connecting the vessel ends representing high inhomogeneities[17].

The assignment of the edge-weights can be analyzed based on the above perspectives. Let $S \subseteq V$ be a nonempty subset of nodes, $i \in S$, and $j \notin S$. Intuitively, the similarity between nodes j and i can be defined as:

$$\phi_S(i,j) = a_{ij} - \frac{1}{|S|} \sum_{j \in S} a_{ij} \tag{2}$$

This measure is with respect to the mean similarity between i and its surroundings in S, and $\phi_S(i,j)$ can be either positive or negative. $\frac{1}{|S|} \sum_{j \in S} a_{ij}$ is the average weighted degree of i with regard to S. It can be observed that $\frac{1}{|S|} \sum_{j \in S} a_{ij} = 0$ for any $i \in V$, and $\phi_{\{i\}}(i,j) = a_{ij}$. For each node $i \in S$, the weight of i with regard to S is assigned as:

$$\omega(i) = \begin{cases} 1 & \text{if } |S| = 1 \\ \sum_{j \in S \setminus \{i\}} \phi_{S \setminus \{i\}}(j,i) \omega_{S \setminus \{i\}}(j) & \text{otherwise.} \end{cases} \tag{3}$$

where $S \setminus \{i\}$ indicates the the nodes set S excluding the node i, and $\omega_S(i)$ demonstrates the overall similarity between node i and the nodes of $S \setminus \{i\}$ with respect to the overall similarity among the nodes in $S \setminus \{i\}$.

Finally, the total weight of S can be calculated by summing $\omega_S(i)$: $W(S) = \sum_{i \in S} \omega_S(i)$. For example, Fig. 3 demonstrates an edge-weighted graph, and we have: $\omega_{1,2,3}(1) = \phi_{2,3}(3,1)\omega_{2,3}(2) + \phi_{2,3}(2,1)\omega_{2,3}(3) = 12$. Similarly, $\omega_{1,2,3}(2) = 0$ and $\omega_{1,2,3}(3) = 12$ are obtained, which yield $W(1,2,3) = 12 + 0 + 12 = 24$.

We define set as a *dominant set* if the set satisfies the following two conditions: 1. $\omega_S(i) > 0$, for all $i \in S$; 2. $\omega_{S \cup \{i\}}(i) < 0$, for all $i \notin S$. It is evident from the above properties that the first condition defining a dominant set is internal homogeneity, whereas the second concerns external incoherence.

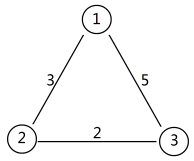

Fig. 3. Edge-weighted graph.

3. EXPERIMENTAL RESULTS

We evaluated the proposed topology estimation method against three publicly available datasets: the Iowa Normative Set for Processing Images of the REtina (INSPIRE)[21], IOSTAR[22], and VICAVR[23] datasets. The INSPIRE dataset has 40 high resolution images, each of 2392×2048 pixels. IOSTAR contains 24 images taken with a scanning laser camera (SLO) each of 1024×1024 pixels. The VICAVR dataset includes 58 images with a resolution of 784×584 pixels each. All of these datasets have manual annotations on artery /vein classification[10, 11, 13], and the IOSTAR dataset also has annotations on vessel bifurcation/crossing. However, none of these three datasets has annotations on vessel topology. Therefore, we asked an expert to manually label the topological information of the vascular structure on all images from these datasets. Each single vessel tree is graded as one color, as shown in middle column of Fig. 4.

The right-hand column of Fig. 4 illustrates the results of our vascular topology estimation method on datasets INSPIRE, IOSTAR, and VICAVR, respectively. Compared with the manual annotations, it reveals that our method is able to trace most vascular structures correctly: only a few crossing points were incorrectly traced, as shown in the middle column of Fig. 4 - the pink squares indicate the significant points which were traced incorrectly. To facilitate better observation of the performance of the proposed method, the accuracy results with regard to different significant points (connecting, bifurcation, and crossing points) are presented individually in Table 1. It may be observed that the method achieved accuracy of 0.915, 0.928, and 0.889 in INSPIRE, IOSTAR, and VICAVR, respectively. The accuracy scores in this table indicate the percentage of the relevant significant points that were correctly handled.

In addition, the results obtained by the proposed vascular topology estimation method were compared with those obtained by five state-of-the-art vascular topology estimation

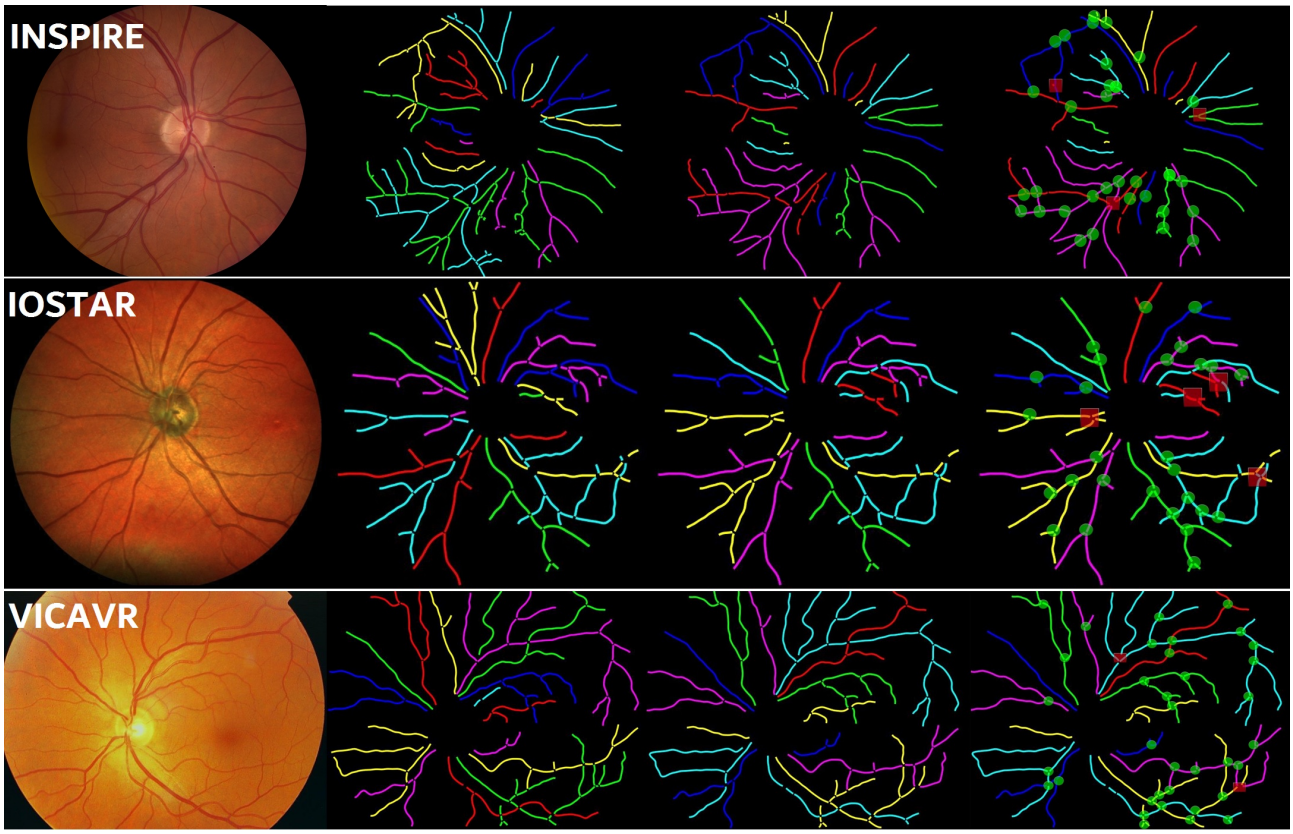

Fig. 4. Examples of vascular topology estimation on retinal datasets INSPIRE, IOSTAR, and VICAVR. From left to right column: original image, manual annotations, the automatic topology estimation results, and correct and incorrect connections are highlighted by green disks and pink squares, respectively.

methods [3, 10, 11, 12, 24] on images from the INSPIRE dataset: the results are shown in Table 2. The results show that our method achieves the best performance, with an accuracy score of 0.883. For the purposes of a fair comparison, the accuracy scores in Table 2. are the percentage of correctly classified vessels' centerline pixels[11].

4. CONCLUSIONS

In this work, we have proposed a novel framework to estimate the topology of retinal vascular trees based on the concept of dominant set clustering. The problem of estimating the topology of vascular trees was formalized as a pairwise clustering problem. It is demonstrated that our method achieves competitive results when compared with existing state-of-the-art methods. It is believed that the proposed method could be a powerful tool for analyzing vasculature for better management of a wide spectrum of vascular-related diseases.

In our future work, we will test our method on other retinal datasets (e.g., RITE[25]) and neuronal datasets (e.g., DIADEM[26]), and the validations will be taken under both connection points-wise and centreline pixel-wise. Furthermore, the estimated vascular topology will be used to support artery / vein discrimination and classification.

Table 1. Performances of the proposed method on vessel tracing at different significant points.

	INSPIRE	**IOSTAR**	**VICAVR**
# connecting points	3,209	1,920	4,678
# correctly detected	3,125	1,874	4,500
accuracy	0.973	0.976	0.960
# bifurcation points	1,998	1,213	2,953
# correctly detected	1,776	1,109	2,501
accuracy	0.889	0.914	0.847
# crossing points	778	482	1210
# correctly detected	574	373	862
accuracy	0.738	0.774	0.712
overall accuracy	0.915	0.928	0.889

Table 2. Performance results on INSPIRE dataset.

	[12]	[11]	[3]	[10]	[24]	ours
accuracy	0.769	0.845	0.773	0.851	0.769	**0.883**

5. REFERENCES

[1] Y. Zhao, Y. Zheng, Y. Liu, J. Yang, Y. Zhao, D. Chen, and Y. Wang, "Intensity and compactness enabled saliency estimation for leakage detection in diabetic and malarial retinopathy," *IEEE Trans. Med. Imaging*, vol. 36, no. 1, pp. 51–63, 2017.

[2] Y. Zhao, I. MacCormick, D. Parry, N. Beare, S. Harding, and Y. Zheng, "Automated detection of vessel abnormalities on fluorescein angiogram in malarial retinopathy," *Sci Rep*, vol. 5, pp. 11154, 2015.

[3] J. De, L. Cheng, X. Zhang, F. Lin, H. Li, K. Ong, W. Yu, Y. Yu, and S. Ahmed, "A graph-theoretical approach for tracing filamentary structures in neuronal and retinal images," *IEEE Trans. Med. Imaging*, vol. 35, no. 1, pp. 257–72, 2016.

[4] R. Estrada, M. J. Allingham, P. S. Mettu, S. W. Cousins, C. Tomasi, and S. Farsiu, "Retinal artery-vein classification via topology estimation," *IEEE Trans. Med. Imaging*, vol. 34, no. 12, pp. 2518–2534, 2015.

[5] J. Cheng, J. Liu, Y. Xu, F. Yin, D. Wong, N. Tan, D. Tao, C. Cheng, T. Aung, and T. Wong, "Superpixel classification based optic disc and optic cup segmentation for glaucoma screening," *IEEE Trans. Med. Imaging*, vol. 32, no. 6, pp. 1019–1032, 2013.

[6] G. Azzopardi, N. Strisciuglio, M. Vento, and N. Petkov, "Trainable COSFIRE filters for vessel delineation with application to retinal images," *Med. Image Anal.*, vol. 19, pp. 46–57, 2015.

[7] Y. Zhao, Y. Liu, X. Wu, S.P. Harding, and Y. Zheng, "Retinal vessel segmentation: An efficient graph cut approach with retinex and local phase," *PLoS ONE*, vol. 10, pp. e0122332, 2015.

[8] M. Fraz, P. Remagnino, A. Hoppe, B. Uyyanonvara, A. R. Rudnicka, C. G. Owen, and S. A. Barman, "Blood vessel segmentation methodologies in retinal images - a survey," *Comput. Meth. Prog. Bio.*, vol. 108, pp. 407–433, 2012.

[9] J. Soares and M. Cree, "Retinal vessel segmentation using the 2D Gabor wavelet and supervised classification," *IEEE Trans. Med. Imag.*, vol. 25, pp. 1214–1222, 2006.

[10] X. Lyu, Q. Yang, S. Xia, and S. Zhang, "Construction of retinal vascular trees via curvature orientation prior," in *IEEE International Conference on Bioinformatics and Biomedicine, BIBM 2016, Shenzhen, China, December 15-18, 2016*, 2016, pp. 375–382.

[11] B. Dashtbozorg, A. M. Mendonça, and A. Campilho, "An automatic graph-based approach for artery/vein classification in retinal images," *IEEE Trans. Image Processing*, vol. 23, no. 3, pp. 1073–1083, 2014.

[12] M. Niemeijer, B. Ginneken, and M. Abramoff, "Automatic classification of retinal vessels into arteries and veins," in *SPIE Medical Imaging*, 2009, vol. 7260, pp. 72601F–1–72601F–8.

[13] M. Niemeijer, X. Xu, A. V. Dumitrescu, P. Gupta, B. van Ginneken, J. C. Folk, and M. D. Abràmoff, "Automated measurement of the arteriolar-to-venular width ratio in digital color fundus photographs," *IEEE Trans. Med. Imaging*, vol. 30, no. 11, pp. 1941–1950, 2011.

[14] M. Martínez-Pérez, A Hughes, A. Stanton, S. Thom, N. Chapman, A. Bharath, and K. Parker, "Retinal vascular tree morphology: a semi-automatic quantification," *IEEE Trans. Biomed. Engineering*, vol. 49, no. 8, pp. 912–917, 2002.

[15] T. Qureshi, A., and B. Al-Diri, "A bayesian framework for the local configuration of retinal junctions," in *2014 IEEE Conference on Computer Vision and Pattern Recognition, CVPR 2014, Columbus, OH, USA, June 23-28, 2014*, 2014, pp. 3105–3110.

[16] R. Estrada, C. Tomasi, S. Schmidler, and S. Farsiu, "Tree topology estimation," *IEEE Trans. Pattern Anal. Mach. Intell.*, vol. 37, no. 8, pp. 1688–1701, 2015.

[17] M. Pavan and M. Pelillo, "Dominant sets and hierarchical clustering," in *9th IEEE International Conference on Computer Vision (ICCV 2003), 14-17 October 2003, Nice, France*, 2003, pp. 362–369.

[18] M. Pavan and M. Pelillo, "Dominant sets and pairwise clustering," *IEEE Trans. Pattern Anal. Mach. Intell.*, vol. 29, no. 1, pp. 167–172, 2007.

[19] Y. Zhao, L. Rada, K. Chen, S. P. Harding, and Y. Zheng, "Automated vessel segmentation using infinite perimeter active contour model with hybrid region information with application to retinal images," *IEEE Trans. Med. Imaging*, vol. 34, no. 9, pp. 1797–1807, 2015.

[20] P. Bankhead, J. McGeown, and T. Curtis, "Fast retinal vessel detection and measurement using wavelets and edge location refinement," *PLoS ONE*, vol. 7, pp. e32435, 2009.

[21] "INSPIRE," `http://webeye.ophth.uiowa.edu/component/k2/item/270`.

[22] "IOSTAR," `http://www.retinacheck.org/`.

[23] "VICAVR," `http://www.varpa.es/vicavr.html`.

[24] V. Joshi, M. Garvin, J. Reinhardt, and M. Abramoff, "Automated method for the identification and analysis of vascular tree structures in retinal vessel network," in *SPIE Medical Imaging*, 2011, p. 79630I.

[25] Q. Hu, M. D. Abramoff, and M. K. Garvin, "Automated construction of arterial and venous trees in retinal images," *Journal of Medical Imaging,*, vol. 2, pp. 044001, 2015.

[26] Todd A. Gillette, Kerry M. Brown, and Giorgio A. Ascoli, "The DIADEM metric: Comparing multiple reconstructions of the same neuron," *Neuroinformatics*, vol. 9, no. 2-3, pp. 233–245, 2011.